Available online at www.sciencedirect.com
ScienceDirect
International Journal of Mass Spectrometry 264 (2007) 53–60
International Journal of Mass Spectrometry
www.elsevier.com/locate/ijms

Mass spectra measured by a fully integrated MEMS mass spectrometer

J.-P. Hauschild*, E. Wapelhorst, J. Müller

Institute of Microsystems Technology, Hamburg University of Technology, Eißendorfer Straße 42, D-21073 Hamburg, Germany

Received 24 January 2007; received in revised form 22 March 2007; accepted 23 March 2007
Available online 27 March 2007

Abstract

Breakthrough measurements of a single chip mass spectrometer are presented. This planar integrated micro-mass spectrometer (PIMMS) is dedicated for mobile measurements, portable applications as well as for continuous process monitoring.

The waferbased fabrication in MEMS technology allows a very cost-efficient mass production. All critical structures are fabricated by a one mask anisotropic deep silicon etch, avoiding alignment difficulties. The small size (5 mm × 10 mm) reduces the vacuum requirements by several orders of magnitude, thus a one stage pumping system can provide the necessary vacuum. The operation is based on electron impact ionization and a synchronous ion shield mass filter.

The electron beam for ionization is supplied by a source, that extracts electrons from a high density microwave plasma. The integrated ion optics extract and focus the beam into the mass separator, where time variant electric fields separate the ions according to their mass-to-charge ratio. An energy filter ensures that the ion beam is monochromatic before it is finally recorded at the detector.

The accomplished experiments prove the concept of the fully integrated mass spectrometer on a chip. Mass spectra of different gas compositions measured with the PIMMS are presented.

Keywords: Micro-mass spectrometer; Plasma electron source; Ion source; MEMS microfabrication; Synchronous ion shield mass separator

1. Introduction

Mass spectrometry is one of the most relevant techniques for chemical and biological analysis and well established in laboratory environments. To apply this technology to portable field applications and in situ measurements, several research projects deal with the miniaturization of mass spectrometers and their components, especially mass separators. In [1] the miniaturization of different types of mass separators in micro-electro-mechanical systems (MEMS) technology is reported.

Ion traps have been proposed in different shapes for the fabrication in micrometer scale by MEMS techniques. An approach to match the field requirements of an ion trap with the restrictions in MEMS technology is shown in [2]. Cylindrical ion traps (CIT) have been fabricated in arrays to use the advantages of miniaturization (e.g., reduced cost, low operating voltage), while keeping the sensitivity at a moderate level [3–6].

Quadrupole mass separators were considered for downscaling by different research groups, because of their simplicity and compactness. Arrays of quadrupole mass separators have been investigated for increased performance [7]. The difficulty of fabricating a perfectly aligned linear quadrupole in MEMS technology has been solved in [8,9]. Self-aligning spring structures in silicon keep the 30 mm long metal rods in their exact position yielding in a good separation performance.

A time-of-flight (TOF) mass spectrometer fabricated by electroplated nickel structures on silicon is presented in [10]. The mass separation is shown for externally ionized sample gas only.

A Wien filter in MEMS is proposed in [11] and adresses the application of low cost helium leak detection. Preliminary results are shown for a microfabricated mass separator using external magnets.

All above mentioned publications have in common that only components of a mass spectrometer have been miniaturized and tested as separate units. This paper presents the miniaturization

* Corresponding author. Tel.: +49 40 42878 2334; fax: +49 40 42878 2396.
E-mail address: jp.hauschild@tu-harburg.de (J.-P. Hauschild).

1387-3806/$ – see front matter © 2007 Elsevier B.V. All rights reserved.
doi:10.1016/j.ijms.2007.03.014

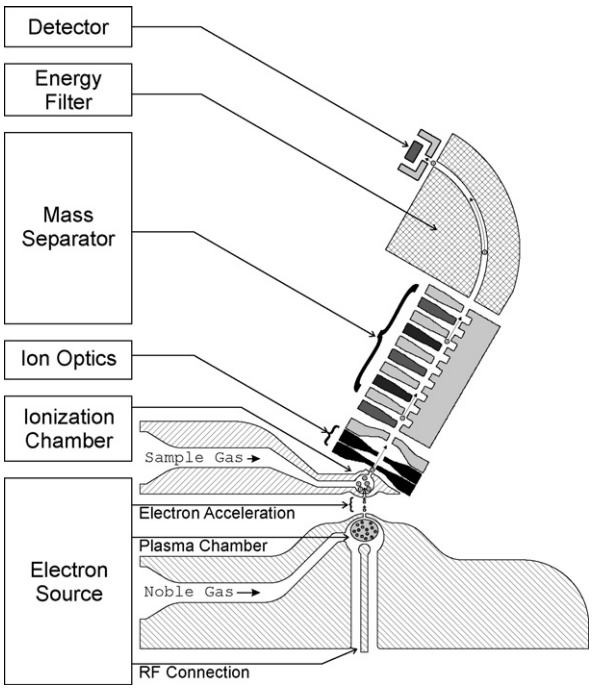

Fig. 1. Schematic view of PIMMS structures.

of a mass spectrometer with all essential components on one chip.

A planar integrated miniaturized mass spectrometer (PIMMS) fabricated by microsystems technology offers several advantages: a wafer based design enables large-scale cost-efficient production [12,13]. All major structures of the PIMMS are fabricated in a single mask anisotropic deep silicon etch process, eliminating the need for alignment of the units to each other. The mass separator length can be reduced to a few millimeters, thus the requirements for the vacuum are relaxed significantly. For a system of this size a vacuum with a pressure of 1 Pa is sufficient, which can be provided by a one stage pumping system or a micro-pump as proposed in [14]. Furthermore, the small dimensions assure a low sample and carrier gas consumption and reduce the response time. Another advantage of miniaturization are the high electric fields that can be generated by low voltages, thus reducing the power consumption and allowing the use of standard integrated circuits to drive the PIMMS. The envisioned size of a complete PIMMS is that of a cell phone, and the expected cost will be a fraction of state of the art devices.

The ability to fabricate low-cost microfabricated mass spectrometers will allow to install dense networks of mass spectrometers for pervasive monitoring in a wide variety of environments. Multiple existing and potential applications like immission monitoring, identification of CFC, surveillance of air contaminations, on site measurements by rescue services, and multiple mass spectrometer networks on chemical plants are feasible.

2. Function principle

The micro-mass spectrometer (Fig. 1) consists of six units: the electron source, the ionization chamber, the ion optics, the mass separator, the energy filter, and the detector. They are described in detail in the following sections.

2.1. Overview

The sample gas is ionized in the ionization chamber by electron impact ionization. The necessary electron beam is provided by the micro-plasma electron source. The ion optics extract the ions and accelerate these to a defined kinetic energy, resulting in an ion beam with a mass dependent velocity distribution. This ion beam enters the mass separator built by a channel of electrode pairs. The signals applied to these electrodes generate a time variant electric field within the channel, facilitating mass separation. The frequency of the applied signals determines the ion mass to be measured, while ions of other masses are deflected. By changing the frequency a large mass interval can be scanned and interrelated to the measured output, to generate the mass spectrum of the sample gas. The energy filter constructed as a 90° sector ensures that only ions with a defined energy are recorded at the detector.

2.2. Electron source

A high current density electron beam at a defined electron energy between 50 and 100 eV, which is necessary for electron impact ionization [15], is extracted from a microwave plasma [16–19]. The microwave excitation of the plasma allows a high charge carrier density, while keeping the ion energy low to prevent ageing of the plasma chamber due to sputtering. The plasma chamber has a cylindrical shape with a diameter of 900 μm and a height of 300 μm. The noble gas is fed into the plasma chamber through a capillary of defined diameter and length. This construction allows to control the pressure inside the plasma chamber at the desired pressure of 50 Pa by manipulating the pressure at the input of the capillary. After ignition of the plasma by a spark discharge, the electrons are extracted through a rectangular aperture by an electric field and accelerated into the ionization chamber. The aperture acts as a pressure stage as well and allows to maintain a low pressure in the electron acceleration area. The energy of the electrons is controlled by the voltage between the plasma and the ionization chamber. The total electron current is 100 μA at a current density of 1 A/cm^2.

2.3. Sample gas ionization

The electron impact ionization is performed in the ionization chamber. The high energy electron beam ionizes the sample gas and fragments molecules [20]. The ion yield curve has a flat maximum at electron energies between 50 and 100 eV [21], therefore the rate of fragmentation can be adjusted while keeping the ion current constant. A capillary of defined length ($l = 10$ cm) and inner diameter ($d = 100$ μm) allows to control the pressure p_0 inside the ionization chamber by the pressure p_v applied to the capillary (see Fig. 2). At steady state, the gas flow pressure product q_{pV}^{aperture} [Pa m^3/s] through one pressure aperture of the area

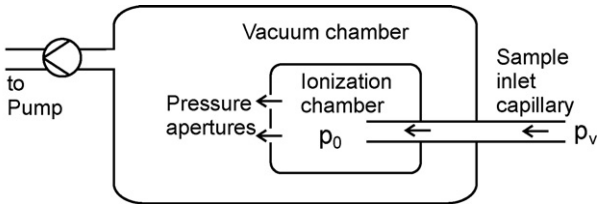

Fig. 2. Pressure scheme of the ionization chamber: the ionization chamber is fed with the probe gas through a capillary and has two outlets, this results in a pressure p_0 in the ionization chamber.

A at a chamber pressure p_0 is calculated as [22]:

$$q_{pV}^{\text{aperture}} = AK_g p_0, \quad \text{with}$$

$$K_g = \left(\frac{2}{\kappa+1}\right)^{1/(\kappa-1)} \sqrt{\frac{2\kappa}{\kappa+1}\frac{RT}{M_{\text{molar}}}}. \tag{1}$$

The adiabatic exponent κ, the gas constant R, and the molar mass M_{molar} depend on the gas. The laminar flow through a capillary with the pressure difference $p_v - p_0$, the length l, and diameter d is given by

$$q_{pV}^{\text{capillary}} = K_c \frac{p_v^2 - p_0^2}{2}, \quad \text{with } K_c = \frac{\pi}{128\eta}\frac{d^4}{l}. \tag{2}$$

At steady state ($q_{pV}^{\text{aperture}} = q_{pV}^{\text{capillary}}$), the positive solution of the quadratic equation, derived from (1) and (2), is the pressure in the ionization chamber

$$p_0 = -\frac{AK_g}{K_c} + \sqrt{\left(\frac{AK_g}{K_c}\right)^2 - p_v^2}. \tag{3}$$

The total ion current strongly depends on the ionization characteristics of the sample gas and the pressure in the ionization chamber. To characterize the ion source, experiments were carried out with different compositions of argon, neon and carbon dioxide. The capillary pressure p_v was controlled by a pressure controller which supervises a set of mass flow controllers (one for each gas). The results are shown in Fig. 3, where the pressure in the ionization chamber is converted by Eq. (3). The ionization maximum of argon is located at a lower pressure than neon, which is attributed to the different electron impact ionization cross-sections [23–25]. The optimum pressure for ionization is lower for larger cross-sections. The carbon dioxide ionization experiment shows two maxima which might result from partial fragmentation.

2.4. Ion extraction optics

The ion optics consist of electrostatic lenses realized by three pairs of electrodes adjacent to the ionization chamber with defined dc potentials applied [26,27]. A 3D finite element method (Femlab®/Matlab®) was used to simulate and optimize the dimensions and the electric potentials of the rectangular shaped apertures.

The electric field between the ionization chamber and the first pair of electrodes (1.25 MV/m) extracts the ions, and the following pairs of electrodes focus and parallelize the ion beam

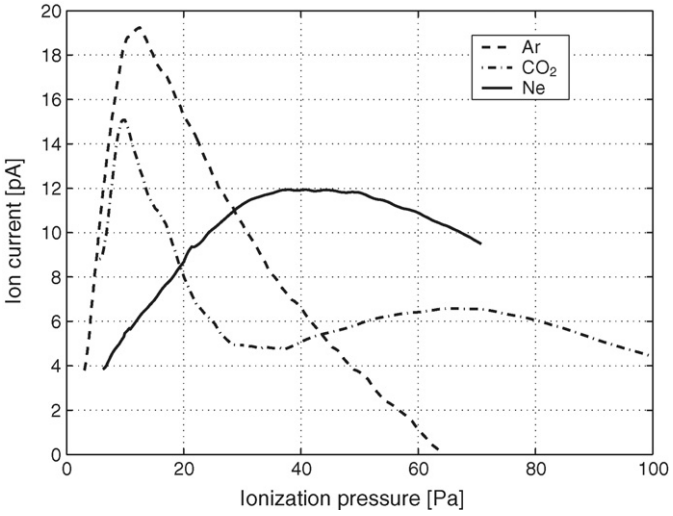

Fig. 3. Ionization experiments with different gases. The graphs show that the ionization cross-section of neon is smaller than for argon or carbon dioxide (maximum shifted to a higher ionization pressure).

as shown in Fig. 4. The negative effect of the ions' energy distribution is minimized by reducing the penetration depth of the electrical field in the ionization chamber. Ions once caught by the electrical field near the outlet aperture leave the ionization chamber immediately. Therefore, all ions experience the same electrical field, and due to the pressure drop at the outlet aperture the ions do not interfere with each other. To address this effect in the simulation, the starting points of the ions were chosen close to the outlet aperture (distance smaller than 100 μm). The electric fields between the following pairs of electrodes form an ion beam which consists of ions of a defined kinetic energy E.

The resulting velocity of the ions v_i depends on their mass m_i as

$$v_i = \sqrt{2\frac{E}{m_i}}. \tag{4}$$

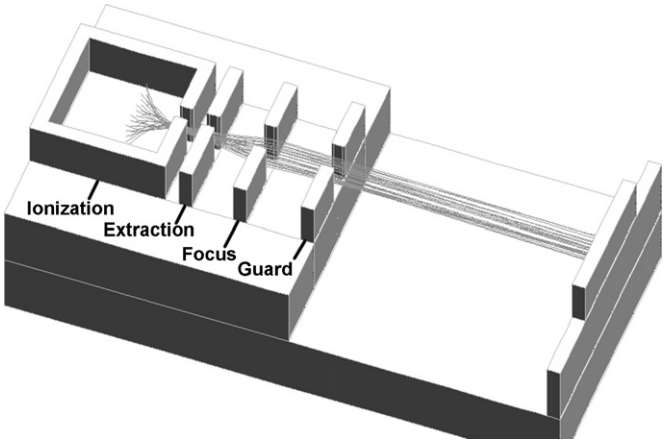

Fig. 4. Ion extraction optics: the voltages U_{extract}, U_{focus}, and U_{guard} are optimized by simulations.

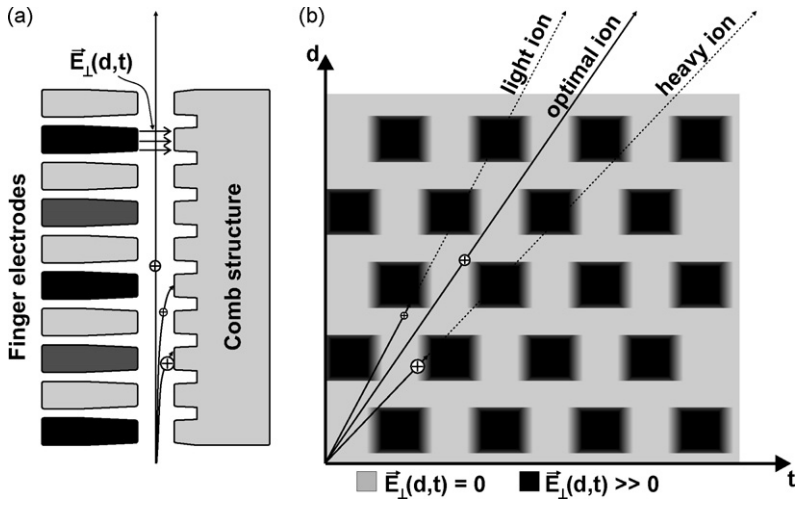

Fig. 5. Function principle of the synchronous ion shield mass filter: (a) mass separator with an injected ion and (b) path-time-field diagram showing $E_\perp$ in the center of the ion channel with respect to time t.

2.5. Synchronous ion shield (SIS) mass separator

The SIS separator is developed from the traveling dipole field mass separator described in [13]. An ion channel is formed by a group of ten electrodes opposite to a comb structure, as shown in Fig. 5 a. Every second electrode and the comb structure are pulled to a defined electric potential leading to field free zones within the channel. Square wave (SW) signals having a defined phase shift are applied to the remaining electrodes. This operation generates a time-variant electric field within the channel perpendicular to the ion path, as sketched in Fig. 5 b, the path-time-field (PTF) diagram. The dark areas denote a strong electric field perpendicular to the ion path, while the bright areas denote a field free region. Field free 'shields' are traveling along the ion channel with a velocity defined by the frequency of the SW signals. Only two SW signals are necessary for operation of this mass separator: signal one is applied to electrodes one, five, and nine. Signal two, which is 180° phase shifted to signal one, is applied to electrodes three and seven.

An ion injected into the mass separator can be plotted on the PTF diagram as a straight line with a velocity dependent slope, see Eq. (4). Fast ions have a steeper slope than slower ones. If the ion speed is synchronous to the traveling field, the ion moves along the channel without being deflected. This is referred to as "synchronous ion shield mass separator" and is also shown in the PTF diagram (Fig. 5b): the line of the ion with the desired velocity remains always in the grey area. Ions having a different velocity will be deflected towards the sidewalls of the channel. In the PTF diagram the straight lines of those ions hit the dark areas denoting a strong field for deflection.

By scanning the frequency of the SW signals a mass range is scanned (Fig. 6). The relation between the frequency f of the SW signal and the relative atomic mass m_{molar} is

$$f = \sqrt{\frac{2E_{\mathrm{kin}}}{d^2 m_{\mathrm{molar}}}} \tag{5}$$

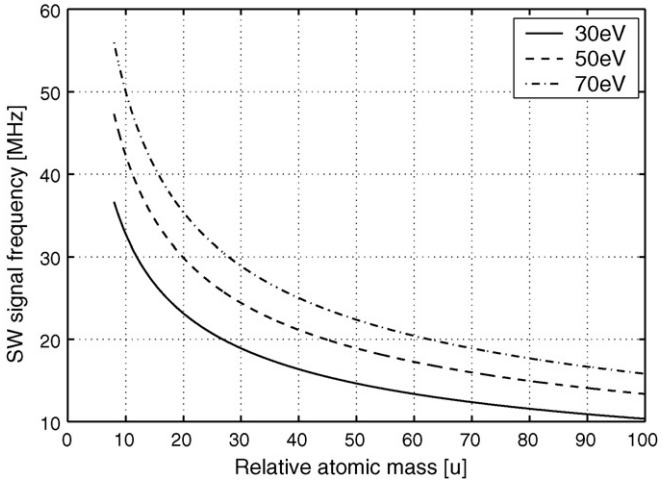

Fig. 6. Relation between SW signal frequency and atomic mass for three different ion energies.

with kinetic energy E_{kin} and distance d between two connected electrodes.

2.6. Energy filter

Ions that are not monochromatic with respect to the desired kinetic energy will pass the mass filter even if their mass differs from the selected one. The deviation of kinetic energy is caused by thermal variation of the start energy and by ions, which pass electrodes during switching. In order to prevent the recording of non-monochromatic ions, an energy filter is placed behind the mass filter.

This electrostatic filter is realized as a 90° sector as shown in Fig. 7. The voltage $U_{90°}$ applied to the 90° electrodes depends on the ion energy E, the ion charge q, and the inner and outer radius of the sector $r_{\mathrm{i}} = r_{\mathrm{m}} - (d/2)$ and $r_{\mathrm{o}} = r_{\mathrm{m}} + (d/2)$, respectively:

$$U_{90°} = 2\ln\left(\frac{r_{\mathrm{i}}}{r_{\mathrm{o}}}\right)\frac{E}{q}. \tag{6}$$

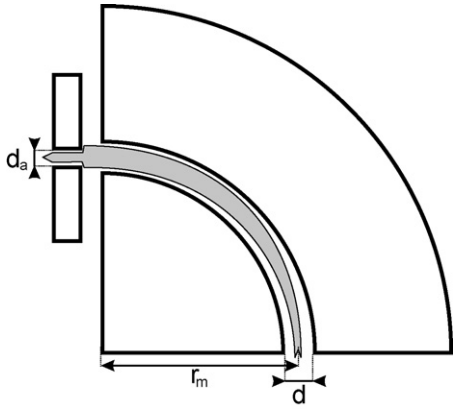

Fig. 7. Filter setup using an electrostatic 90° sector with an inlet width d, outlet width d_a, and the radius r_m.

Fig. 8 shows that the calculated filter voltage fits the experimental results. The bandwidth $\Delta E/E$ depends on the aperture width d_a at the end of the energy filter and is calculated from

$$\frac{\Delta E}{E} = \frac{d_a}{r_m}. \quad (7)$$

The energy distribution of the ions varies in the range of a few eV (e.g., 5–10 eV). Fig. 9 illustrates that d_a should be smaller than 100 μm to achieve clear peaks in the mass spectrum with $E_{kin} = 30$ eV, $r_m = 1500$ μm and $d = 100$ μm. A smaller aperture d_a will sharpen the peaks of the mass spectrum, but the total ion current will decrease.

2.7. Detector

The detector is a faraday cup without suppressor electrodes. This simple electrode arrangement catches all ions and neutralizes them. The ion energy is kept low in the whole system, thus the loss of ions due to reflection at the surface of the detector electrode is negligible.

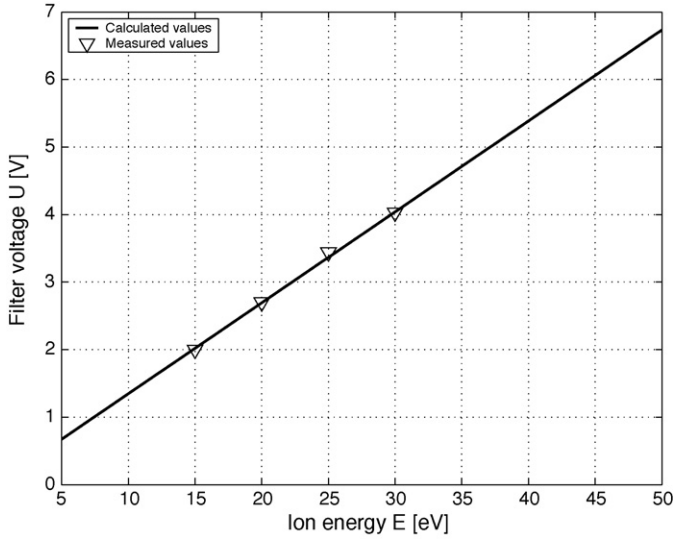

Fig. 8. Voltage between the filter electrodes for the 90° sector with $d = 100$ μm, $d_a = 100$ μm, and $r_m = 1.5$ mm. The triangles show measured values.

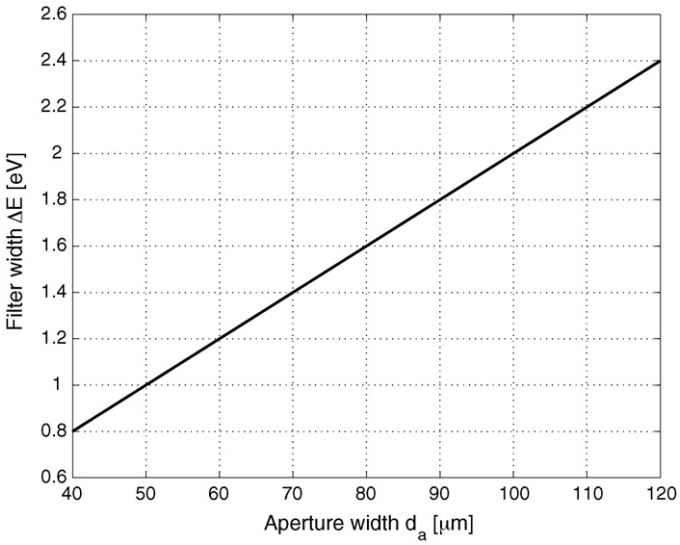

Fig. 9. Filter width ΔE for different aperture widths d_a at an ion energy of $E = 30$ eV.

For increased sensitivity a secondary electron multiplier (SEV) will be integrated in the future. The idea is to fabricate electrodes to form a voltage cascade supplied by a metal thin film resistor. Depending on the surface coating of the electrodes a voltage of $U_{step} = 200$–300 V [28] is necessary to operate the secondary electron multiplier. Limiting factor for the number of amplifier steps is the maximum voltage which can be applied to the system without electrical breakdown over the gap between two electrodes or over the surface of the isolating substrate. A realistic amplification of a SEV integrated in the PIMMS is $v \approx 1000$ at 4–6 multiplication steps.

2.8. Vacuum system

The vacuum requirements of a mass spectrometer can be described by the mean free path length ($\bar{l}_{ion}$) of the ions with the radius r_{ion} in air (r_{gas}).

$$\bar{l}_{ion} = \frac{1}{n\pi(r_{gas} + r_{ion})^2}, \quad (8)$$

with

$$n = \frac{p}{kT}. \quad (9)$$

At a pressure p of 1 Pa and at room temperature ($T = 300$ K) the mean free path length of Ar ($r_{ion} = 98$ pm) in air ($r_{gas} = 370$ pm) is $l_{ion} = 6.02$ mm [22]. The calculations show, that the pressure required to run the PIMMS should be 1 Pa or lower to separate even larger molecules. In the future it is planed to use a micro-pump to generate the required vacuum.

The working principles of micro-pumps can be classified in displacement and dynamic pumps [29]. The displacement pumps use a diaphragm, rotor or piston to pump the medium which is a gas or liquid. Most of this displacement pumps are designed to transport liquids and are unfeasible for the use as a vacuum pump. Some examples of displacement vacuum pumps are given in [30,31]. The most convenient micro-vacuum pump

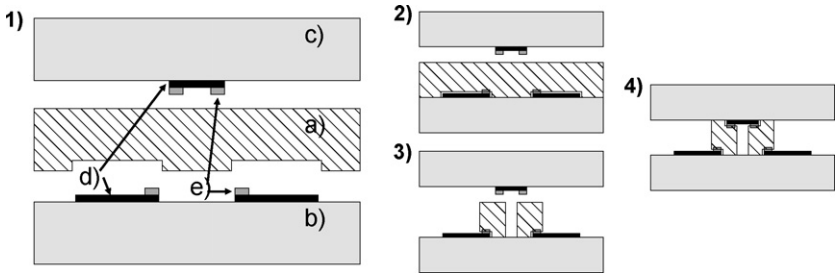

Fig. 10. Fabrication steps: (a) silicon, (b) bottom glass, (c) top glass, (d) nickel conductors and (e) gold pads.

for the PIMMS seems to be the jet pump which is a dynamic pumping principle. One example of a vapor jet pump is shown in [14]. However, non of the described pumps is able to reach the required pressure of 1 Pa up to now, but the theoretical considerations show, that this goal is reachable in the future. Instead of using a micro-pump a conventional one stage vacuum pump can be used to reduce cost and size of the vacuum system.

3. Fabrication

The fabrication based on MEMS standard processes is a major advantage of the presented PIMMS [32]. The fabrication in MEMS technology is very cost-efficient: all processes are applied to hundreds of systems on one substrate at the same time by transferring the pattern using lithography and etching.

All units of the mass spectrometer are integrated planar on one chip, and the critical structures are fabricated in a one mask anisotropic deep reactive ion etch (DRIE) process. In order to achieve free standing silicon structures, the DRIE process is applied to a sandwich of a borosilicate glass (500 μm thick) and a highly conductive silicon (300 μm thick) substrate. The glass carries also nickel conductors to contact the free standing electrodes. The actual contact is made from gold which alloys with the silicon during bonding. To avoid a mechanical contact between the nickel conductors and the silicon, a recess with a depth of 500 nm is etched into the silicon before the wafers are bonded. A second borosilicate glass substrate is bonded on top of the silicon structures to enclose the functional components and provide additional electrical contacts.

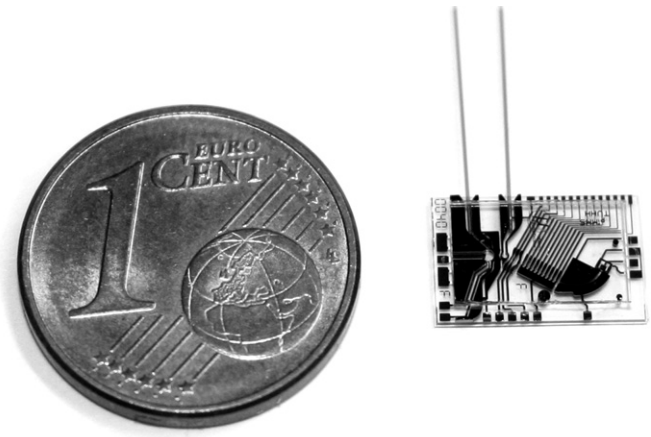

Fig. 11. Photo of the PIMMS chip with two capillaries for noble gas and probe gas.

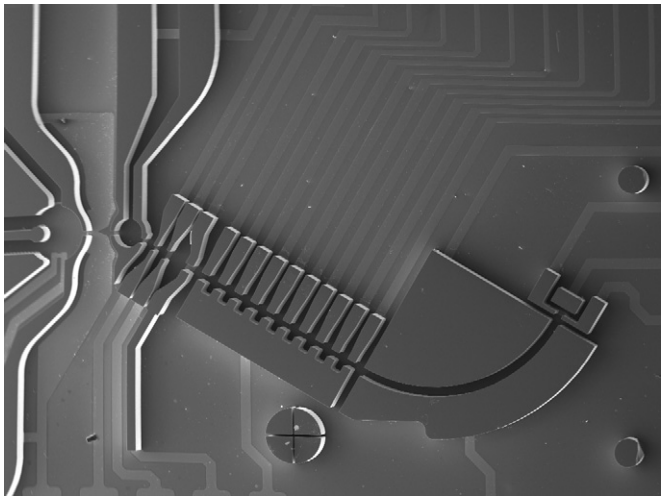

Fig. 12. SEM image of the PIMMS showing all essential structure.

In step one (Fig. 10(1)) the nickel conductors with gold pads at the contact areas on top of both glass substrates are patterned, and the cavities are etched into the silicon substrate. In step two (Fig. 10(2)) the silicon wafer is bonded to the bottom glass wafer. In step three (Fig. 10(3)) the silicon is etched by a DRIE process [33,34], followed by bonding the second glass substrate on top of the silicon structures (Fig. 10(4)) The processed substrate is diced to finalize the fabrication of about 100 micro-mass spectrometers.

Fig. 11 shows one PIMMS chip with all components integrated. The decisive structures and the electrical circuit on the bottom glass substrate of the PIMMS are shown in the SEM image in Fig. 12.

4. Measurements

Experiments were carried out with sample gases of different compositions of argon, neon, nitrogen, carbon dioxide, and air. The measurement conditions are shown in Table 1. The gas composition is supplied by a group of mass flow controllers supervised by a pressure controller in order to maintain a constant pressure in the ionization chamber. The detector current is

Table 1
Measurement conditions for the mass spectra in Figs. 13–15

Component	Parameter	Value
Electron source	Noble gas	Ar
	Pressure	50 Pa
	RF frequency	2.5 GHz
	RF power	2 W
	Electron energy	100 eV
Ion source	Sample gas	Ar, Ne, N_2, CO_2, Air
	Pressure	50 Pa
	Electric potential	30 V
Ion optics	Extraction electrode potential	$-95V$
	Focus electrode potential	12 V
	Guard electrode potential	0 V
Mass separator	SW signal frequency	10–35 MHz
	SW signal duty cycle	30%
	SW signal amplitude	10 V
Energy filter	Outer electrode potential	2.19 V
	Inner electrode potential	$-2.19V$
Detector	Detector electrode potential	0 V

measured with respect to the frequency of the SW signal and afterwards converted by Eq. (5). Fig. 13 shows the mass spectra of two compositions of argon, neon and nitrogen. The mass spectrum of only Ar and Ne shows, that argon ionizes far better than neon. The added nitrogen can clearly be identified in form of a strong peak at mass 28 u (N_2^+) and a smaller peak at mass 14 u (the fragment N^+). The mass spectra shown in Fig. 14 are measured with Ar, Ne, and CO_2. These measurements show that a mass of 44 u (CO_2^+) can clearly be separated from a mass of 40 u (Ar^+). The fragments of CO_2 (C^+, O^+, CO^+) are also apparent in the spectra.

Fig. 15 depicts a spectrum of lab air, where nitrogen, oxygen, and fragments (N^+, O^+) are visible.

These results proof the concept of a fully integrated mass spectrometer in MEMS technology.

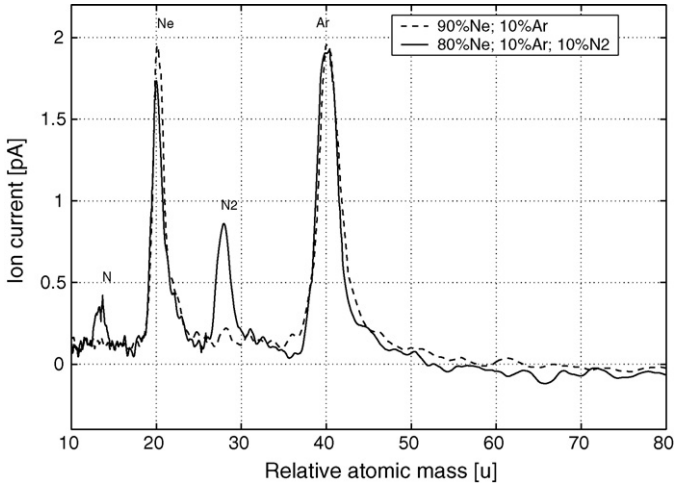

Fig. 13. Mass spectrum of Ar and Ne measured under the conditions shown in Table 1.

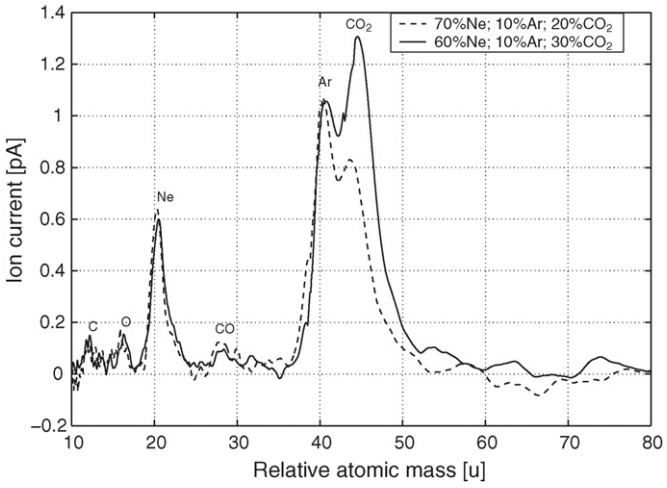

Fig. 14. Mass spectrum of CO_2 measured under the conditions shown in Table 1.

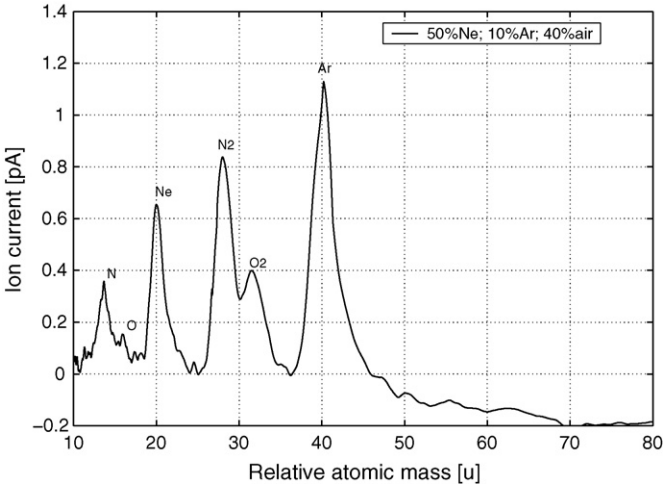

Fig. 15. Mass spectrum of air measured under the conditions shown in Table 1.

5. Conclusion

The experiments show the initial performance of the micro-mass spectrometer presented in this paper. All components, i.e., electron source, ion source, and mass- and energy filter, have been integrated on one chip, with the essential structures fabricated by a few standard MEMS processes.

The mass separation of the PIMMS will be further improved by optimizing the filter geometry and the ionization characteristics, as well as by optimizing the DRIE process for the PIMMS, to reduce the feature size of the silicon structures. Furthermore, an integrated secondary electron multiplier will be incorporated to increase the sensitivity.

Acknowledgement

This work was funded by Deutsche Forschungsgemeinschaft (DFG).

References

[1] E.R. Badman, R.G. Cooks, J. Mass Spectrom. 35 (2000) 659.
[2] M.J. Madsen, W.K. Hensinger, D. Stick, J.A. Rabchuk, C. Monroe, Appl. Phys. B (2004).
[3] H. Peddanenikalava, K. Potluri, S. Bhansali, R.T. Short, D. Fries, A microfabrication strategy for cylindrical ion trap mass spectrometer arrays, in: Proceedings of IEEE Sensors, Orlando, FL, IEEE, 2002.
[4] J. Maxam, P.T.A. Reilly, W.B. Whitten, J.M. Ramsey, Rapid Commun. Mass Spectrom. 18 (2004) 721.
[5] S. Pau, C.S. Pai, Y.L. Low, J. Moxom, P.T.A. Reilly, W.B. Whitten, J.M. Ramsey, Phys. Rev. Lett. 96 (2006) 120801.
[6] M.G. Blain, L.S. Riter, D. Cruz, D.E. Austin, G. Wu, W.R. Plass, R.G. Cooks, Int. J. Mass Spectrom. 236 (2004) 91.
[7] S. Boumsellek, R.J. Ferran, Am. Soc. Mass Spectrom. 12 (2001) 633.
[8] S. Taylor, R.F. Tindall, R.R.A. Syms, J. Vacuum Sci. Technol. B 19 (2) (2001) 557.
[9] M. Geear, R.R.A. Syms, S. Wright, A.S. Holmes, J. Microelectromech. Syst. 14 (5) (2005) 1156.
[10] H.J. Yoon, J.H. Kim, E.S. Choi, S.S. Yang, K.W. Jung, Sens. Actuators A 97–98 (2002) 441.
[11] N. Sillon, R. Baptist, Sens. Actuators B 83 (2002) 129.
[12] V. Relling, Untersuchungen zum Aufbau eines Mikromassenspektrometers, in: Dissertation, Hamburg University of Technology, Germany, 1997.
[13] P. Siebert, G. Petzold, A. Hellenbart, J. Müller, Appl. Phys. A67 (1998) 155.
[14] M. Doms, J. Müller, Sens. Actuators A 119 (2005) 462.
[15] J.H. Gross, Mass Spectrometry, first ed., Springer Heidelberg, 2004.
[16] G. Petzold, P. Siebert, J. Müller, A micromachined electron beam ion source, in: Proceedings μ TAS 2000, Enschede, Netherlands, 2000, p. 171.
[17] A. Feustel, J. Müller, V. Relling, A microsystem mass spectrometer, in: Proceedings μ TAS 1994, Enschede, Netherlands, 1994, p. 299.
[18] G. Petzold, P. Siebert, J. Müller, Sens. Actuators B (67) (2000) 101.
[19] J.-P. Hauschild, E. Wapelhorst, J. Müller, M. Doms, in: Proc. of 9th μ TAS Conference, vol. 1, Transducer Research Foundation, Boston, MA, USA, October 2005, p. 476, ISBN 0-9743611-1-9.
[20] H. Budzikiewicz, Massenspektrometrie, Eine Einführung, fifth ed., Wiley-VHC Weinheim, 1998.
[21] F. Aulinger, G. Franke, K. Habfast, H. Kienitz, G. Spiteller, Massenspektrometrie, Verlag Chemie GmbH, 1968.
[22] M. Wutz, H. Adam, W. Walcher, Theorie und Praxis der Vakuumtechnik, fifth ed., Vieweg Verlag, 1992.
[23] T.D. Märk, G.H. Dunn, Electron Impact Ionization, Springer, 1985.
[24] W. Lotz, Z. Phys. 216 (1968) 241.
[25] W. Lotz, J. Opt. Soc. Am. 58 (1967) 236.
[26] I.G. Brown, The Physics and Technology of Ion Sources, second ed., Wiley-VCH, 2004.
[27] H. Zhang, Ion Sources, Springer, Tokyo, 1999.
[28] M. von Ardenne, Deutscher Verlag der Wissenschaften 1 (1962).
[29] D.J. Laser, J.G. Santiago, J. Micromech. Microeng. 14 (2004) R35.
[30] R. Rapp, W.K. Schomburg, D. Maas, J. Schulz, W. Stark, Sens. Actuators A 40 (1994) 57.
[31] Z. Cui, C.G. Takoudis, Design and simulation of a vaccum micropump, in: Microfluidics BioMEMS, SPIE, 2001, p. 263.
[32] M.J. Madou, Fundamentals of microfabrication: the science of miniaturization, 2nd edition, CRC Press LLC, 2001.
[33] A.A. Ayon, R. Braff, C.C. Lin, H.H. Sawin, M.A. Schmidt, J. Electrochem. Soc. 146 (1999) 339.
[34] A.A. Ayon, X. Zhang, R. Khanna, Sen. Actuators A 91 (2001) 381.